9-25-2020

A Review on the Biodistribution, Pharmacokinetics and Toxicity of Bismuth-Based Nanomaterials

Samireh Badrigilan

Fatemeh Heydarpanahi

Jalal Choupani

Mehdi Jaymand

Hadi Samadian

See next page for additional authors

Authors

Samireh Badrigilan, Fatemeh Heydarpanahi, Jalal Choupani, Mehdi Jaymand, Hadi Samadian, Mojtaba Hoseini-Ghahfarokhi, Thomas J. Webster, and Lobat Tayebi

International Journal of Nanomedicine

Dovepress
open access to scientific and medical research

Open Access Full Text Article

REVIEW

A Review on the Biodistribution, Pharmacokinetics and Toxicity of Bismuth-Based Nanomaterials

This article was published in the following Dove Press journal:
International Journal of Nanomedicine

Samireh Badrigilan[1,*]
Fatemeh Heydarpanahi[2,*]
Jalal Choupani[3,4]
Mehdi Jaymand[5]
Hadi Samadian[5]
Mojtaba Hoseini-Ghahfarokhi[1,5]
Thomas J Webster[6]
Lobat Tayebi[7]

[1]Department of Radiology and Nuclear Medicine, School of Paramedical Sciences, Kermanshah University of Medical Sciences, Kermanshah, Iran; [2]Department of Toxicology and Pharmacology, School of Pharmacy, Mazandaran University of Medical Sciences, Sari, Iran; [3]Department of Medical Genetics, School of Medicine, Tabriz University of Medical Sciences, Tabriz, Iran; [4]Immunology Research Center, Tabriz University of Medical Sciences, Tabriz, Iran; [5]Nano Drug Delivery Research Center, Health Technology Institute, Kermanshah University of Medical Sciences, Kermanshah, Iran; [6]Department of Chemical Engineering, Northeastern University, Boston, MA 02115, USA; [7]Marquette University School of Dentistry, Milwaukee, WI 53233, USA

*These authors contributed equally to this work

Correspondence: Mojtaba Hoseini-Ghahfarokhi; Lobat Tayebi
Email m.hoseini@kums.ac.ir; lobat.tayebi@marquette.edu

Abstract: Here, bismuth-based nanomaterials (Bi-based NMs) are introduced as promising theranostic agents to enhance image contrast as well as for the therapeutic gain for numerous diseases. However, understanding the interaction of such novel developed nanoparticles (NPs) within a biological environment is a requisite for the translation of any promising agent from the lab bench to the clinic. This interaction delineates the fate of NPs after circulation in the body. In an ideal setting, a nano-based therapeutic agent should be eliminated via the renal clearance pathway, meanwhile it should have specific targeting to a diseased organ to reach an effective dose and also to overcome off-targeting. Due to their clearance pathway, biodistribution patterns and pharmacokinetics (PK), Bi-based NMs have been found to play a determinative role to pass clinical approval and they have been investigated extensively in vivo to date. In this review, we expansively discuss the possible toxicity induced by Bi-based NMs on cells or organs, as well as biodistribution profiles, PK and the clearance pathways in animal models. A low cytotoxicity of Bi-based NMs has been found in vitro and in vivo, and along with their long-term biodistribution and proper renal clearance in animal models, the translation of Bi-based NMs to the clinic as a useful novel theranostic agent is promising to improve numerous medical applications.

Keywords: bismuth nanoparticles, biocompatibility, pharmacokinetic, biodistribution and clearance

Introduction

Bismuth-based nanomaterials (Bi-based NMs) hold great potential as theranostic agents due to their high atomic number (Z= 83), X-ray sensitive capabilities, near-infrared driven semiconductor properties, and low cost. These characteristics have been used to develop theranostic platforms for tumors and vascular computed tomography (CT)[1,2] as well as photoacoustic (PA)[3,4] imaging approaches, drug delivery,[5,6] radiation therapy (RT),[7,8] photothermal (PTT)[6,9] and photodynamic (PDT)[10,11] therapeutic modalities.[12] All administrated exogenous materials, as diagnostic or therapeutic agents, should be entirely cleared from the body within a satisfactory time after injection, according to the requirements as reported by the US Food and Drug Administration (FDA).[13] Despite effective contrast signal enhancement and tumor inhibition triggered by Bi-based NMs, their biocompatibility and easy excretion from the body are major characteristics that minimize the possible risks associated with the interactions of Bi-based NMs within biological systems.

submit your manuscript | www.dovepress.com
DovePress
http://doi.org/10.2147/IJN.S250001

Once injected, NPs are transferred by the bloodstream to target tissues and different organs. In the meantime, immunological mechanisms start a cohort of processes to eliminate these foreign particles from the body.[14] Therefore, highly active clearance mechanisms affect the expected distribution of Bi-based NMs in different organs. The travelling pattern of Bi-based NMs in different organs or tissues is determined by their physicochemical properties, principally considered as the biodistribution and the rate of NP recognition and elimination via metabolism, the immune system and excretion referred to as pharmacokinetics (PK).[15]

Biodistribution and PK are key points to maximize the expected therapeutic functionality of Bi-based NMs and to minimize side effects in any clinical or diagnostic application.

Besides, the toxicity of Bi-based NMs on living organisms is an important factor that limits their biomedical applications. Bi-based NM induced-toxicity depends on their concentration, duration of interaction with living matter, biological stability, and their accumulated dose in tissues and organs.[16] For future clinical translation, understanding the underlying biodistribution and clearance mechanisms of Bi-based NMs is a primary step.

For the first time, this review paper provides a narrative view on the in vivo biological barriers encountered by Bi-based NMs. The parameters that play key roles in the clearance pathways, body distribution and ultimate fate of Bi-based NMs are discussed to design agents based on Bi-based NMs of high biosafety and significant diagnostic and therapeutic efficacy for future biomedical applications.

Toxicity

Free types of heavy metal elements are very toxic, thus, their bio-elimination from the body is an important issue that should be carefully considered in their design for medical applications. Bi has been introduced as the only heavy metal that is almost non-toxic.[17] Bi compounds are generally considered as safe heavy metals compared to its neighboring elements, such as mercury (Hg), thallium (Tl), and lead (Pb). Also, unlike other heavy metals like gold and platinum, Bi is not stable in the body and is anticipated to slowly decompose into soluble Bi (III)[18] thus, their fast excretion from the body is a challenge for their use in clinical applications. Dissolved Bi (III) ions from BiNPs are cleared via a cysteine-rich protein in kidneys (called metallothionine) and are excreted by the urine. It has been shown that Bi reacts with this protein earlier than other elements, regardless of pH.

Bi (III) compounds have been used for many centuries in the medical field, so it is thought that their ions are also safe in biological conditions.[19] A concentration of 50 μg Bi (III)•mL^{-1} has generally been considered as a maximum biocompatible plasma concentration. For more than three centuries, different compounds of Bi (III) (such as colloidal bismuth subcitrate (CBS, De-Nol), bismuth subcitrate potassium (Pylera), bismuth subsalicylate (Helidac) and ranitidine bismuth citrate (RBC, Pylorid, Tritec)) have clinically been used for some gastrointestinal disorders, of which a daily dose can even increase to several grams.[20,21] Also, Bi can eradicate *Helicobacter pylori* in peptic ulcers, syphilis, and tumors and reduce renal toxicity caused by cisplatin.[22] For patients suffering from various stomach diseases, a high dose of up to ~ 4.2 g of bismuth subsalicylate is frequently prescribed, demonstrating the in vivo biosafety of bismuth below acceptable levels of toxicity.

In vitro Toxicity

Cell Viability

The MTT (3-(4,5-Dimethylthiazol-2-yl)-2,5-diphenyltetrazolium bromide) assay is a convenient colorimetric approach for measuring cellular metabolic activity, which can be used as a sensitive indicator of cell viability and proliferation. Based on published evidence, the cytotoxicity of Bi-based NPs (such as bismuth selenide (Bi_2Se_3), bismuth sulfide (Bi_2S_3), copper bismuth sulphide (Cu_3BiS_3), and pure Bi NPs) is insignificant against various cell lines even at high concentrations.[3,5,6,18,23-35] In the case of Bi_2S_3, Liu et al[36] have evaluated the cytotoxicity of Bi_2S_3 NPs in a panel of different cell lines, including lung adenocarcinoma A549 cells, human embryonic kidney 293 cells (HEK293), umbilical vein endothelial cells (HUVEC), and hepatocarcinoma (HepG2) cells. They found that Bi NPs induced minimal toxicity in HepG2 and HUVEC cells, representing negligible cytotoxicity on the human liver and blood vessels. The viability of A549 cells was 78% at the highest concentration of 160μg/mL, which indicated trivial cytotoxicity on lung cells. In contrast, HEK293 cells showed a dose-dependent vulnerability to Bi_2S_3 NPs. A concentration of 20 and 160μg/mL of Bi_2S_3 NPs decreased the viability of HEK293 cells down to 80% and 50% of controls, respectively. Therefore, kidney cells showed the most vulnerability to Bi_2S_3 NP-induced cytotoxicity which was related to the release of

Bi ions. The team also showed that Bi_2S_3 NP-treatment prompted the expression of microtubule-associated protein light chain 3 (LC3) in HEK293 cells, which highlighted autophagy-dependent mechanisms of Bi_2S_3 NPs cytotoxicity. Rabin et al[37] have also reported a median lethal dose (LD_{50}) for U937 cells in the presence of 8 mM free Bi ions, while a LD_{50} value was achieved at a concentration of 100 mM Bi in PVP- Bi_2S_3 NPs (BPNPs). For HepG2 hepatocarcinoma cells, the LD_{50} value of Bi^{3+} ions and BPNPs was 5 mM and 114 mM, respectively. It is desirable that the LD_{50} value of the NPs be higher than the required dose (ED) for their respective applications. The ED/LD_{50} profile for U937 cells treated with BPNPs was similar to that observed for an iodinated agent, while a superior profile was found for HepG2 cells.[37]

Besides, Bi-based NMs can directly cause oxidative stress injury by disruption on mitochondrial and lysosomal function. Mahmoud et al[38] used kidney (NRK-52E), liver (HepG2), lung (A549) and intestine (Caco-2) cell lines to evaluate the cytotoxicity of Bi_2O_3 NPs and found that the half-maximal inhibitory concentration (IC_{50}) was 96.55, 35.11, 59.08, and 93.55μg•mL^{-1}, respectively. They found that the level of malondialdehyde (MDA) and 8-hydroxydeoxyguanine (8-OHdG) increased while glutathione (GSH) levels decreased due to Bi_2O_3-induced cytotoxicity, proving disrupted function of mitochondria and lysosomes. Furthermore, the cell vulnerability to genotoxic damage induced by Bi_2O_3 NPs was ranked as NRK-52E > Caco-2 > HepG2 > A549. For two other types of Bi-based NMs,[39,40] it been shown that a concentration of 100 μg Bi.mL^{-1} can induce cytotoxicity in half of human skin-derived (HaCaT) cells by provoking oxidative stress mechanisms, disturbing the cell cycle, and induction of apoptosis. In contrast, several reports found no evidence regarding the cytotoxicity of Bi-based NPs even at high doses. A high dose of 3 mg Bi ·mL^{-1} in Bi_2S_3[41] and bismuth ferrite (BFO)[10] NPs achieved a viability over 80% against HeLa and HepG2 cells, respectively. Furthermore, doses of 100 mg mL^{-1} and 0.932 mg•mL^{-1} of Bi_2O_3 NPs induced no cytotoxicity in murine periodontal ligament and rat osteosarcoma cells and monkey kidney cells, respectively.[42,43]

The maximum safe doses of Bi-based NMs after 24h of incubation are listed in Table 1. As shown, no cytotoxicity effect was observed for both normal and tumoral cells after 24h of incubation with doses of 400 to 15,000 μg•mL^{-1} of all these Bi-based NMs.

Hemolytic Effect

For in vivo biomedical applications of NPs, blood-compatibility is a critical test that should be investigated to determine the hemolytic capability of NPs when exposed to blood components. As a result, nanoprobes with a high degree of hemolysis are not suitable for introduction into the physiological environment. According to the ASTM E2524-08 standard, red blood cell (RBC) damage from foreign agents introduced into the body are significant when the degree of hemolysis reaches 5%. The results reported for Bi-based NMs revealed excellent blood compatibility with a hemolysis effect lower than 2%,[1,2,4,6,34,35,46,47,54,58,66] even at a high concentration of 800 μg•mL−1.[3]

In Ovo Toxicity

The toxicity of Bi_2O_3/HSA core-shell NPs was tested on fertilized eggs of the Gallus chicken. Aviv et al poked a small hole in an egg air sac and injected the solutions directly over the permeable air sac membrane with a hypodermic syringe in the third day of embryonic development. After 14 days, the number of alive chicken embryos in the groups injected with Bi_2O_3 NPs with and without a human serum albumin (HAS) shell were similar to that of the untreated group, indicating high biocompatibility of Bi NPs. Also, the doxorubicin injected embryos was considered as a positive group.[71]

In vivo Toxicity

In vivo Toxicity in Caenorhabditis Elegans

Caenorhabditis elegans (*C. Elegans*) is a well-known model organism that has been commonly used in the field of biology. As a small, free-living, nematode worm, it is one of the simplest organisms with a neural structure, which includes a battery of sense organs. It is a multicellular eukaryote with simple digestive, reproductive and nervous systems, which in its simplicity makes it a great model for a detailed study in cell differentiation, development, neurology and genetics. Interestingly, its transparency facilitates the study of cell differentiation simultaneously allowing optical imaging of its structure. These characteristics make it an outstanding model for evaluating nanomaterial toxicity.

The bright field images show the uptake of Bi_2S_3 @SiO_2 NRs by *C. Elegans*.[72] When following 18 days after co-cultivation of *C. Elegans* with different doses of Bi_2S_3@SiO_2 NRs, no observable proliferation inhibition was found in the *C. Elegans*. Additionally, no noticeable

Table 1 The Maximum Safe Doses of Bismuth-Based Nanomaterials After 24h of Incubation

Nanomaterials	Cell Lines	Dose (μg• mL^{-1})	References	Nanomaterials	Cell Lines	Dose (μg• mL^{-1})	References
Cu_3BiS_3	4T1	200	29	Bi	HeLa	500	18
	HeLa	200	44		U937	10,000	37
	MCF-7				HepG2		
	HUVEC*	100	45		MCF-7	400	46
	BEL-7402				SMMC-7721		
					VSMC		
	HeLa	200	31		4T1	200	47
	L929*				HUVEC*		
	HeLa	600	5		U14	500	1
	MCF-7	150	48		4T1	400	32
					L02*		
	HeLa	200	49		4T1	160	50
					NIH-3T3		
					HUVEC		
Bi_2Se_3	4T1	200	26		HeLa	500	34
	3T3*				MCF-7		
	MCF-7	200	51		HeLa	600	23
	HeLa	400	3		HeLa	300	4
	HUVEC*				HUVEC*		
	H22	200	52		4T1	100	53
	BEL-7402	100	7		HeLa	400	30
	HeLa	200	8	Bi_2S_3	4T1	300	24
	HeLa	200	54		4T1	160	28
BiFe	BJ5ta*	100	27		HeLa	300	2
	HepG2				HUVEC*		
	HeLa	500	34		4T1	15,000	55
	MCF-7				J774		
	HepG2	3000	10		HeLa	7500	41
Bi_2S_3/Au	4T1	100	56	Bi_2S_3/G	HUVEC*	40	6
	MCF-7				HeLa		
					MCF-7		
					HepG2		
					BEL-7402		
$FeSe_2/Bi_2S_3$	4T1	200	9		PC3	200	25
BiSe/G	HeLa	150	33	BiOCl	MCF-7	200	57
GdBi	C6	200	58		L929	500	59
	COS-7*						
Bi_2WO_6	HeLa	800	11	Bi_2O_3:Yb^{3+}/Er^{3+}	HeLa	1000	60
	HUVE	400	61	Bi_2S_3/FeS_2	4T1	800	62
	HeLa						
GBi	HeLa	500	35	BiOI	HeLa	4200	63
	MCF-7						
BMS	HUVE	200	64		4T1	200	65
	HeLa				HeLa		

(*Continued*)

Table 1 (Continued).

Nanomaterials	Cell Lines	Dose ($\mu g \cdot mL^{-1}$)	References	Nanomaterials	Cell Lines	Dose ($\mu g \cdot mL^{-1}$)	References
$K_{0.3}Bi_{0.7}F_{2.4}$	HeLa	500	[66]	$(BiO)_2CO_3$	Huh-7	5mM	[48]
BiOBr	L929	1000	[67]	Bi_2S_3-MnO_2	U14	10	[68]
$AgBiS_2$	UMR-106	500	[69]	BPZP	4T1	100	[70]

Note: * The cells are non-cancer cells.

Abbreviations: 3T3, mouse embryonic fibroblast; 4T1, breast cancer cell; $AgBiS_2$ NPs, silver bismuth sulfide; BEL-7402, liver carcinoma cell; BJ5ta, human fore skin fibroblast; Bi, pure bismuth; Bi_2S_3, bismuth sulfide; Bi_2Se_3, bismuth selenide; Bi_2S_3/Au, bismuth sulfide-gold; Bi_2S_3/G, bismuth sulfide-graphene; Bi_2S_3-MnO_2 NPs, bismuth sulfide and manganese oxide nanocomposites; Bi_2WO_6, bismuth tungstate; BiFe, bismuth ferrite; $(BiO)_2CO_3$, bismuth subcarbonate; BiOBr, bismuth oxybromide; BiOCl, bismuth oxychloride; BiOI, bismuth oxyiodide; BMS NRs, bismuth sulfide -mesoporous silica; BPZP, bismuth sulfide-linked zinc protoporphyrin; BiSe/G, bismuth selenide-graphene; C6, glioma cell; COS-7, monkey kidney fibroblasts; Cu_3BiS_3, copper bismuth sulfide; $FeSe_2/Bi_2S_3$, iron diselenide-bismuth selenide; GBi, graphene-bismuth; GdBi, gadolinium-bismuth; H22, hepatic carcinoma cell; HeLa, cervical cancer cell; HepG2, hepatic carcinoma cell; Huh-7, human liver cell; HUVEC, human umbilical vein endothelial cell; J774, Mus muscles reticulum cell sarcoma; L02, human hepatic cell; L929, murine fibroblast cell; MCF-7, breast cancer cell; PC3, human prostate carcinoma; SMMC-7721, hepatic carcinoma cell; U14, cervical carcinoma cell; U937, macrophage cells; VSMC, vascular smooth muscle cell.

effect on their worm body length in comparison to the group with any treatment was induced, therefore there was not any toxicity mediated by Bi_2S_3@SiO_2 NRs for the *C. Elegans*. After three days, the auto-fluorescence intensity in the worm intestine in the control group was similar as those exposed to different concentrations of Bi_2S_3 @SiO2 NRs, which could be attributed to the negligible effect of NRs on the lipofuscin level.

In vivo Toxicity in Zebrafish

The zebrafish (*Danio rerio*) is a commonly used animal model in a variety of biological sciences due to its unique features, such as well characterized embryonic stages, a completely sequenced genome with high similarity to the human genome, high rate of fecundity and rapid development and affordable husbandry. Also, they have similar features and mechanisms of behavior to mammalian models in toxicology, which make them a suitable model for toxicity testing.

After treatment with bismuth–asparagine coordination polymer spheres (BACP-2),[73] a significant deformation was observed in zebrafish morphology including shortened body length and head diameter (particularly eyes), but it was highest at 28 postfertilization (hpf). In addition, at 52 and 72 hpf, an observable pericardial edema was found compared with the un-injected embryos (Figure 1A). However, a recovery of the BACP-2 mediated effects was found by embryos at 100 hpf. Also, alcian blue staining revealed that the BACP-2 had no effect on cartilage development (Figure 1B).

Cellular movement and cell fate determination are two vital processes for the normal formation of organs. The expression of krox20 (Egr2) has no significant difference in rhombomeres (r) 3 and 5 between the two groups. However, due to the narrower space between r3 and r5 in all of the injected embryos, it is evident that the BACP-2 injection leads to a decrease in the size of the hindbrain. The different expression levels of otx2—as a marker in the development process of the forebrain, midbrain and eyes—induced the abnormal small-eye phenotype in the embryos. Analysis of cardiac myosin light chain 2 (cmlc2) expression as a heart-specific marker revealed that BACP-2 caused defects in heart development in zebrafish embryos. Also, the abnormal cell migration and slow growth of the treated embryos resulted from the dysregulation in the expression of not tail (ntl). Overall, these results indicated that BACP-2 impaired normal embryonic head and heart development in zebrafish (Figure 1C).

In vivo Toxicity in Murine Models

The rats and mice, known as murine models, are commonly used to investigate the in vivo toxicity induced by NPs. The histological analysis, physical and behavioral signs, hematological parameters and blood biochemistry analysis, and immunotoxicity are considered as major factors for toxicity assessment in the case of such mammalian models. In this subsection, toxicity index factors and related studies will be described in detail.

Physical and Behavioral Signs

Bodyweight, litter size, and behavior traits such as eating, drinking, and mating, all can be monitored to measure the in vivo toxicity profile of a NP, and deviation from the control case usual reflects a physiology disorder. In the case of Bi NPs, the impact of toxicity on the physical function of the body has

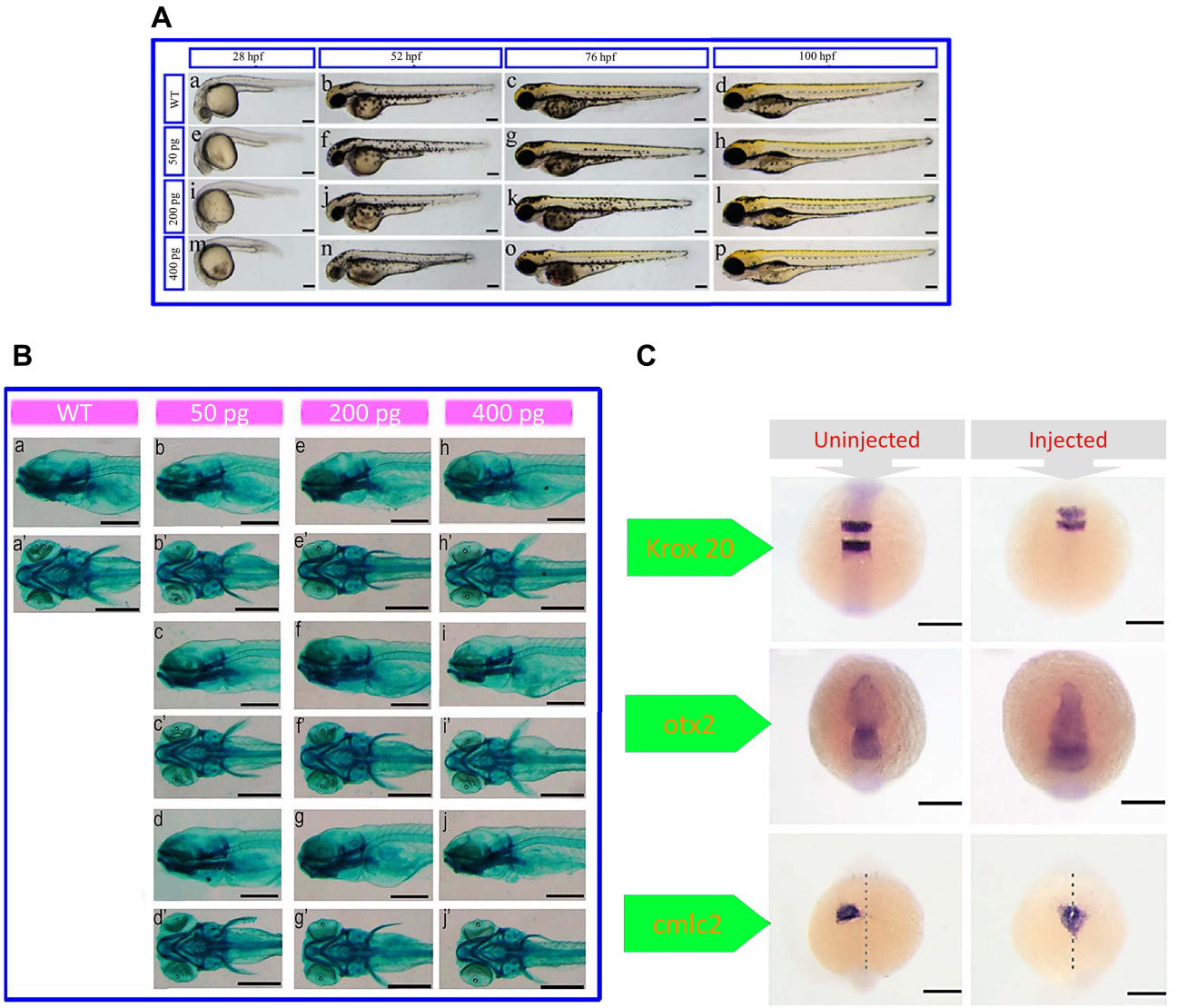

Figure 1 (**A**) Morphological features of embryos injected with different concentrations of bismuth–asparagine coordination polymer spheres (BACP-2) at different times post-fertilization. (**B**) Alcian blue staining of BACP-2 effect on cartilage growth at 5 hours postfertilization (hpf) (a-j: lateral view; a'-l': ventral view).(**C**) . Expression of krox20 (at 12 hpf), orthodenticle homeobox 2 (otx2) (at 12 hpf) and cardiac myosin light chain-2 (cmlc2) (at 24 hpf) genes in uninjected embryos and embryos after injection with 400 pg of BACP-2. Reprinted with permission from He N, Li X, Feng D, et al. Exploring the toxicity of a bismuth–asparagine coordination polymer on the early development of zebrafish embryos. *Chem Res Toxicol.* 2013;26(1):89–95.[73] Copyright 2013 American Chemical Society.

only been physically evaluated by monitoring changes in the bodyweight of treated animals (rats or mice). The weight lost-triggered by various types of Bi NPs has been investigated with no important changes in comparison to controls. Specifically, as a model, a 90 day follow-up of the intraperitoneally injection of Bi_2Se_3 NPs (20 mg/kg) into C57 male mice[8] revealed that polyvinylpyrrolidone coated bismuth selenide nanoparticles (PVP-Bi_2Se_3 NPs) were not able to induce any significant harmful effects on mice growth, and there was no statistically meaningful difference in mice body weight in comparison to the control mice. In addition, it has been reported that no obvious abnormal behavior was observed after treatment, indicating physically and behaviorally excellent in vivo compatibility of PVP-Bi_2Se_3 NPs.

Histology

For histopathological analysis, major organs (typically the liver, lung, spleen, heart, and kidney) are harvested from the animal models exposed to the nanoprobes, placed in a formalin solution, embedded in paraffin, sectioned into tiny slices, stained with hematoxylin and eosin (H&E) and, finally, an optical microscope was employed to observe possible cell damages, including tissue death, lesions, and inflammation.

In all histological in vivo toxicity assessments of Bi NPs with various shapes, coatings and compounds, the major organs (heart, liver, spleen, lung, and kidney) from the experimental animals showed no/low tissue damage and maintained normal physiological properties. All histological results indicated general innocuity of Bi to induce abnormal histological changes in the organs. After treatment with the PVP-Bi_2Se_3 NPs,[8] no increase in the immune response was found in the thymus of mice during the 90 day experiment; in contrast, the spleen index grew steadily during the first 30 days, then declined with time. No damage signs and pathological lesions were found in the spleen and kidney organs during the course of treatment, but a slight pathological change after injection of the PVP- Bi_2Se_3 NPs was observed in the liver. A 90 days follow-up study revealed a recovery mechanism within the damaged organs to the normal state. The other organs (such as the heart, lung, testis, bladder, and brain) revealed no toxicity index signs during the 90 days. A high aggregation degree of the PVP-Bi_2Se_3 NPs as dark spots with a size smaller than 1 μm was observed in spleen optical images on days 1 and 7, but they disappeared after 90 days.

Hematology and Blood Biochemistry

In the complete blood panel analysis, very important hematology markers including RBC, white blood (WBC) and platelet (PLT) counts, hemoglobin (HGB) concentration, mean corpuscular volume (MCV), mean corpuscular hemoglobin (MCH) concentration, mean corpuscular hemoglobin concentration (MCHC), and hematocrit (HCT) are monitored to investigate the overall physiological health after administration of NPs into the body. Blood biochemistry analysis was employed to investigate the liver and kidney function by measuring markers corresponding to the liver (such as alanine transaminase (ALT), aspartate transaminase (AST) and alkaline phosphatase (ALP) activities) and the kidneys (such as serum levels of albumin (ALB), blood urea nitrogen (BUN), creatinine (CREA) and globulin (GLOB)).

The measurement of typical hematological parameters, such as WBC and RBC counts, did not indicate any significant differences in PVP-Bi_2Se_3 NP-treated mice, compared with the untreated group. However, the increased PLT count returned to the normal level after 90 days of treatment.[8] These results demonstrated that PVP-Bi_2Se_3 NPs have low toxicity in mice. Blood chemistry parameters in the injected group had no signs of a direct effect. The injected NPs had infraction with important proteins in serum, such as albumin, fibrinogen, and insulin. After 1-day of treatment with the PVP-Bi_2Se_3 NPs, no observable differences were measured in all parameters compared to the control group. Meanwhile, a large fraction of the PVP-Bi_2Se_3 NPs accumulated in the liver site during the first day but did not induce serious damage at this time point. On day 7, compared to that of day 1, the change of ALT content was significant for the NP-treated mice, unlike AST and CREA. The ALT level reached a normal state after 90 days of treatment, which could be due to the slight hepatic damage induced by the Bi_2Se_3 NPs during the first 7 days and the damage recovery with more time. Hematological and blood biochemical analyses of the Bi_2Se_3 NP[8] injected mice showed no obvious irregularities in hematological and organs physiological functions. The in vivo coagulation studies showed that the Bi NPs cannot induce any significant change in the levels of fibrinogen (FIB), prothrombin time (PT), thrombin time (TT) or activated partial thromboplastin time (APTT) within blood plasma in comparison to the control plasma.

The reported results showed normal metabolism in all of the major organs of the experimental animals, and there was no significant abnormal body function after exposure to the Bi NPs. The same results have been reported for the in vivo safety of Bi-based NMs in previous studies.[3,4,29,61,62,74,75]

Clearance Pathways

Elimination of undesirable materials from the body, namely excretion or clearance, plays a critical role in biological processes, which potentially helps to prevent damage and toxicity. Clearance of agents through the renal (urine) and hepatic (bile to feces) pathways are considered as two major excretion routes.[76]

Renal clearable agents are a better choice, as they are able to be quickly removed from the body; therefore, slight cellular internalization and metabolism will occur. So, it is a common method to reduce exposure of the body to such agents. The shape, surface charge, and size of materials are major factors for the excretion of these agents through the urinary system based on glomerular filtration in the kidneys.[76] The typical filtration-size threshold (FST) of capillary walls of the glomerulus is about 6 nm, indicating that the filtration of materials with hydrodynamic diameters (HDs) larger than the FST is not possible by the kidneys. When a non-renal clearable substance is introduced into the body, they remain

in the blood circulation and are swallowed by phagocytosis cells such as kupffer cells. These cells are resident macrophages in the reticuloendothelial system (RES) that identify and phagocytose foreign antigens and matters (>10 nm) in the blood to remove them from the body. RES, as a part of immune system, are found throughout the body, mainly in the spleen, liver and other reticular connective tissues, where the exogenous materials are metabolized and removed by the hepatic pathway. In hepatic excretion, the liver is responsible for metabolism and biliary excretion and finally, the foreign materials are excreted in feces. The hepatic route with a complex pathway and longer retention time than the renal route increases the risk of health; therefore, renally excreted probes are better to choose for clinical applications.

Biodistribution Profile and Clearance Pathway of Nanoprobes

In an in vivo system, molecular agents with different structures, properties, and functions behave similarly showing a non-specific distribution, short distribution time, short residence time in blood circulation and almost complete renal clearance within a short-time.[76] The probes, based on a small molecule with a smaller size than FST, do not experience any interactions with serum proteins in the blood; they remain intact and enter into urine after filtration by the glomerular capillary walls (Figure 2A). Hepatic clearance is another elimination route of exogenous agents from the body, which acts almost as a dominant excretion route in the case of nanoprobes and some of the molecular probes with the binding of serum proteins. While the molecular probes can be almost completely excreted via the renal and/or hepatobiliary pathway during a nearly short period of several hours or few days, nanoprobes flow out of the blood circulation and significantly accumulate in organs with reticular and endothelial characteristics for a long time (Figure 2B).

In a physiological medium, the HDs of the most developed Bi NPs are larger than what can pass through the capillary walls and enter urine (~ 6–8 nm). Their large HDs can be attributed to two major reasons. First, their actual size is larger than FST, here's a list, spherical Bi NPs (74 nm),[18] Cu_3BiS_3 hollow nanospheres (80 nm),[5] bismuth sulfide nanorods (diameter of 10 nm and length of 50 nm),[24] bismuth selenide spherical-sponge NPs (125 nm),[3] $FeSe_2$- Bi_2Se_3 nanosheets (thickness of ≈2.6 nm and average diameter of ≈100),[9] rGO/Bi_2S_3 nanocomposites (average diameter of ~100 nm and thickness of ~1.2 nm),[6] and Yb^{3+}/Er^{3+}-codoped Bi_2O_3 nanospheres (350 nm).[60] Second, the size of the nanoprobes becomes dramatically larger in a biological environment (even some with a core size smaller than 6 nm), because their surface coating and adsorption of serum proteins increase—for example, the core size of Bi_2S_3 NPs is 6.1 nm, but the HD of BSA-stabilized Bi_2S_3 NPs increases to 39.52 nm.[28] The HD of BiOI NPs with a core size of 2.6 is ~16 nm.[63] A polyvinylpyrrolidone (PVP) coating increased the size of Bi nanodots form 2.7 nm to 11 nm.[1]

The liver and spleen are predominately the organs that accumulate very large Bi nanoprobes (HD > 400 nm), with > 90% of the injected dose (% ID), and a low concentration of Bi is excreted by the urine (~ 5%ID). The kidney uptake of Bi NPs with a size close to the FST (~ 10 nm) is still significantly lower than those measured for the liver and spleen.[1,77] It was found that the size of the nanoprobes acts as a dominant factor in the filtration efficiency and elimination via the hepatic route. The type of coating is considered as another factor in hepatic clearance.

To date, Bi NPs have been widely coated by a polymer such as PVP, dextran, bovine serum albumin (BSA), human serum albumin (HSA), Tween or polyethylene glycol (PEG).[3,4,11,27,29,55,56,78] The variety of serum proteins present in the blood reaches 300 different types, which forms a diverse protein corona and interacts with the high energy surface of the particle. The increase in the HDs and macrophage uptake by RES organs mainly is due to the type, bioactivity, and concentration of serum protein adsorption to NPs.[79,80] The PEG polymer, as the surface coating, is commonly used to prolong blood retention time and reduce uptake by RES organs of Bi NPs; in contrast, the large HDs of the generated NPs do not allow for renal clearance, maybe with fine control of the PEG density on the Bi NPs surface, the PEGylated-Bi NPs can be cleared via the urinary system. The PEG polymer with a molecular weight of about 500–2000 canform a coiled conformation resistance to protein binding.

Almost all of the developed Bi NPs follow a non-renal clearance profile and demonstrate liver homing ability in the range of 8 ~ 70% ID•g^{-1} at 1 ~ 24 h p.i. with any shape, hydrodynamic size (larger than FST), surface coating, and chemical composition, while the reported dose in the liver and spleen for molecular probes was ~ 0.1–1.0 % ID•g^{-1},[76] (~ 10–1000 times smaller). The reduction of NP core size and also the development of a protein-adsorption

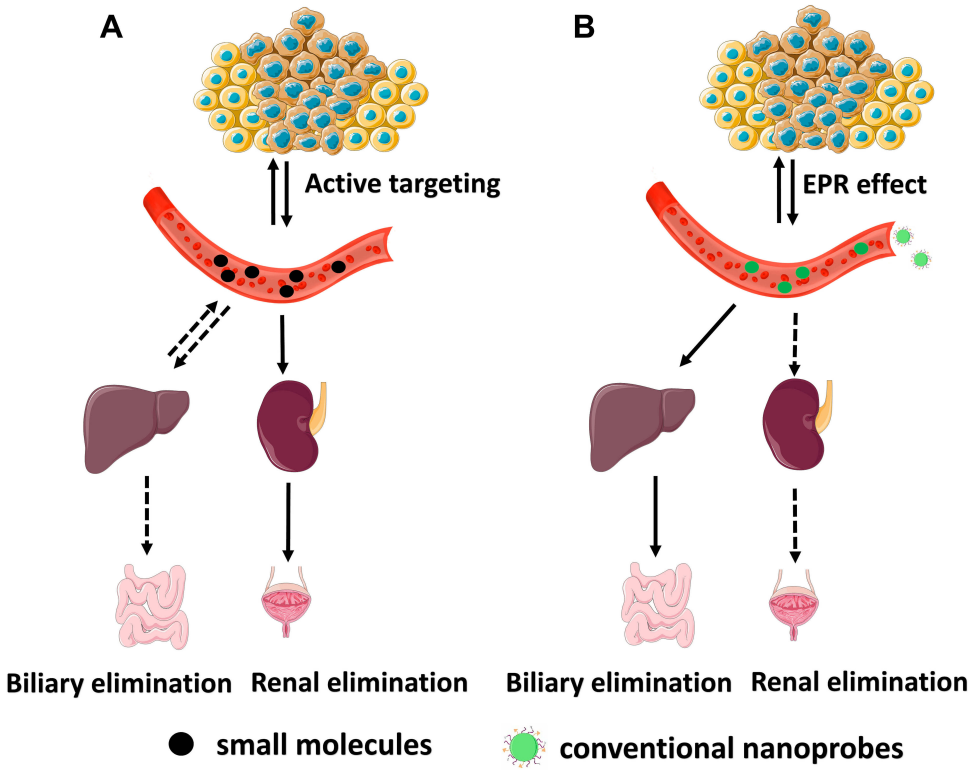

Figure 2 In vivo behavior of (**A**) small molecules and (**B**) conventional nanoprobes after intravenous administration.

-resistant coating on the NP surface mainly help to achieve higher urinary clearance efficiency of Bi NPs. But this strategy is not always feasible, since NPs exhibit size-dependent properties and size reduction may compromise the desired properties and even could vanish following the reduction of particle sizes to less than ~ 5 nm. Also, the synthesis of ultrasound microcapsules/NPs with a size of less than 5 nm is impossible. To maintain NP optical properties for cancer imaging and therapy, accelerating the elimination of NPs of a large size from the body and the development of larger degraded nanoprobes is an alternative. To date, a few degradable NPs based on Bi have been reported. The Bi-based nano compounds are mainly in the form of Bi/Fe, Bi_2Se_3, Bi_2S_3 and Cu_3BiS_3, and the biodegradation mechanisms of each type are fully described in the following section.

In the case of Fe/Bi NPs,[27] the concentration of Bi in the kidney clearly was higher than that measured for Fe 2 h after injection of the Bi–Fe_3O_4 nanocomposites (BION), while their content in the other major organs was almost similar. This shows that the Bi element could be cleared efficiently through the urinary route, due to the degradation of BION in the acidic environment. Such higher levels of Bi in the kidneys and urine, compared with Fe, could be attributed to the confiscation of released Fe ions by ferritin for the synthesis of hemoglobin, whereas there is no such system for the consumption of released Bi ions in the body, allowing for the kidney filtration of free Bi ions. In contrast, after the first incubation of the BION in a 10% FBS solution for 1 h, a reduction in the size from 98 to 90 nm was observed; as time passed to 24 h, the size of BION surprisingly was found to be 48 nm, supporting the supposition of BION degradation. Also, the release test indicated that the amount of Bi and Fe after 4 h in the lysosomal- and blood-mimicking fluid was 80% and 19%, respectively.

In the case of Bi_2Se_3 NPs,[8] the Bi_2Se_3 nanoprobes can be degraded and release Bi and Se ions into the biological environment, providing for renal excretion. The liver, spleen, and kidneys are predominately the homing sites for nanoplates (lateral size of 53.8 nm and thickness size of 4 nm, HD= 59.8 nm), followed by the bladder and testes. The Bi_2Se_3 nanoplates undergo a fast oxidation process in the bloodstream. As a result, the oxidized and intact nanoplates are absorbed by organs containing phagocytic cells, and in contrast, the released Se ions remain in blood circulation for a long time and are excreted via

the urinary system. The Bi- accumulated level in all organs decreased as time increased to 90 days, indicating time-dependent clearance effects. Interestingly, the downward trend of the amount of Se continued for 30 days, whereas the significant level of Se in the kidneys, testes, and bladder was visible 90 days after administration.

In another sample, the renal excretion was the main excretion mechanism on the first day for Bi in the Bi_2Se_3 NPs modified by selenocysteine and polyvinylpyrrolidone (PVP Bi_2Se_3@Sec NPs),[7] while such a mechanism did not exist for Se ions, indicating efficient renal clearance of Bi. It should be noted that the liver, as a major site to synthesize selenoenzymes and selenoproteins, converts Se derivatives to selenoproteins via reduction and methylation reactions. Doran suggested the methylation mechanism of selenium as follows: in the methylation process of SeO_3^{2-}, Se0 could be considered as a starting substrate or the intermediate product of methylation; selenite (IV), as a precursor of selenium integrated into selenoproteins, forms hydrogen selenide (H_2Se) through reduction and methylation mechanisms. Therefore, it is not surprising that released Se ions from Bi_2Se_3@Sec NPs significantly accumulated in the liver.

In the case of Cu_3BiS_3 NPs:[48] The kidneys are the major organ contributing to the metabolism of Tween-Cu_3BiS_3 nanodots (core size of 10 nm, HD ~ 22 nm), and the liver and spleen are next. The Cu_3BiS_3 NDs were fully degraded and metabolized and were excreted from the whole body within a relatively short time. The content of nanodots in the kidneys increased to 35% ID•g^{-1} in the first 2 h, reached a maximum (45% ID•g^{-1}) at 6 h post-injection, and then decreased to 22% ID•g^{-1} at 24h. In contrast, the ND level was as high as 25% ID•g^{-1} and 34% ID•g^{-1} in the liver, 6% ID•g^{-1} and 23% ID•g^{-1} in the spleen after 2 and 6 h, respectively, while in the rest of the organs (heart, lungs, stomach, and intestine), lower than 4% ID•g^{-1} was found. After 1 day, it decreased to 7% ID•g^{-1} in the liver and 11% ID•g^{-1} in the spleen. The in vivo distribution and clearance behaviors of Cu_3BiS_3 NDs were consistent with the acquired CT images at different times (Figure 3A). During 10 min, the contrast of the liver and kidneys was remarkably enhanced, indicating the quick elimination of Cu_3BiS_3 NDs via the urinary system. As time increased to 6 h, the liver had the strongest signal and the spleen was visible, while the bladder was filled with Cu_3BiS_3 NDs. Up to 2 h after injection, the nanoprobes were almost exclusively removed via fecal excretion, as renal clearance gradually took over as the dominate clearance system, so that the efficiency of renal excretion was almost 2-times and 3-times higher than fecal excretion 6 h and 24 h after injection, respectively (Figure 3B).

In biological conditions, the nonstable Cu^+ ions easily undergo an oxidation process and react with ligands like Cl^-, S^{2-} thiols, peptides, and proteins. The degradation and

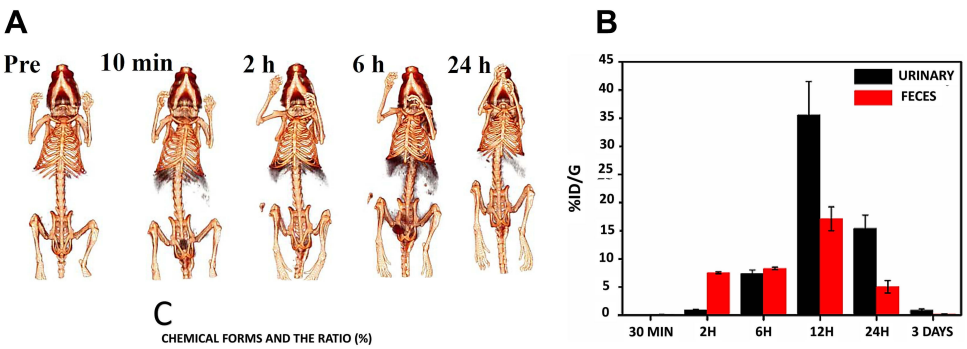

C

CHEMICAL FORMS AND THE RATIO (%)

	Cu_2S	CuS	$CuCl_2$	CuCl	Cu-(R-COO-)	CuO	Cu foil
Cu_3BiS_3 NDs	100	0	0	0	0	0	0
ALF 30 min	40	0	0	22.5	37.5	0	0
ALF 12 h	37.4	0	0	17.9	44.7	0	0
ALF 24 h	0	2.5	6.7	0	90.8	0	0
DI water 2 month	20.6	12.6	0	0	46.7	20	0

Figure 3 (**A**) Computed tomography (CT) images of mice before and after injection of Cu_3BiS_3 NDs at different time points. (**B**) The excretion profiles of Cu_3BiS_3 NDs in mice at different time points. (**C**) Time-dependent copper species from degraded Cu_3BiS_3 NDs in deionized (DI) water. Reprinted with permission from Liu J, Wang P, Zhang X, et al. Rapid degradation and high renal clearance of Cu3BiS3 nanodots for efficient cancer diagnosis and photothermal therapy in vivo. *ACS Nano*. 2016;10(4):4587–4598.[48] Copyright 2016, American Chemical Society.

metabolism mechanism of Cu_3BiS_3 NDs in a biological environment is proposed as follows (Figure 3C). For Cu in an acidic medium, mimicking the lysosomes, nine species exist—Cu, CuS, Cu_2S, $CuCl_2$, CuCl, Cu_2O, CuO, Cu $(CH_3COO^-)_2$, and Cu citrate (in forms of Cu^+ and Cu^{2+})—which are considered as the reference forms to find the chemical behavior of Cu_3BiS_3 NDs in an environment mimicking the body. In the artificial lysosomal fluid (ALF), the Cu_3BiS_3 NDs are gradually converted into a Cu-COO- species. In ALF, the NDs rapidly degrade and form a Cu_2S type with a level of 40% within a half-hour, while none was found after one day due to a quick degradation process for Cu_3BiS_3 NDs. On the other hand, CuCl served as a middle type between Cu_2S and Cu-COO species, given that no steady ratio for CuCl was found. After one day, the level of CuS or $CuCl_2$ species was detected to be 2.5% and 6.7%, respectively, whereas the Cu-COO level was 90.8% in an ALF solution. In contrast, after 60 days in the DI water solution, the Cu_3BiS_3 NDs were converted to Cu_2S (20.6%), Cu-COO- (46.7%) and CuS (12.6%), and a predictable CuO (20%) type was oxidized in a non-acidic environment.

The novel $(BiO)_2CO_3$ nanoclusters (BNCs) assembled into extended and hollow $(BiO)_2CO_3$ nanotubes (BNTs) showing a high renal clearance efficiency in vivo during a short time (Figure 4A).[81] Importantly, the large size BNTs (HD=98 nm) reconverted to the disassembled small BNCs (core size of 1.5 nm) in a slightly acidic medium, such as the tumor environment. The TEM images of the incubated tumor cells showed a shortened length of BNCs in cells, confirming the degradation of the tubular assembly (Figure 4B). The disassembled BNCs easily passed renal filtration and were cleared via the urinary system (Figure 4C). Within 12h, the excreted Bi content via the renal route was measured to be ~36%; interestingly, this amount was lower than 1% for the fecal route.

Pharmacokinetics (PK)

When foreign substances (either drug or contrast agent) enter into the body, their interaction with each of the body organs is a critical issue. The absorption, distribution, metabolism, and excretion (ADME) are four types of main processes defined as PK (Figure 5A). It should be noted that the concentration of exogenous agents in systemic blood circulation is mostly relevant to their accumulated dose in the body. Consequently, to investigate the PK behavior of a probe, the measurement of its blood concentration at different time points is necessary following the injection of a dose, as long as the substance is removed in the body (elimination phase). The main PK parameters—such as

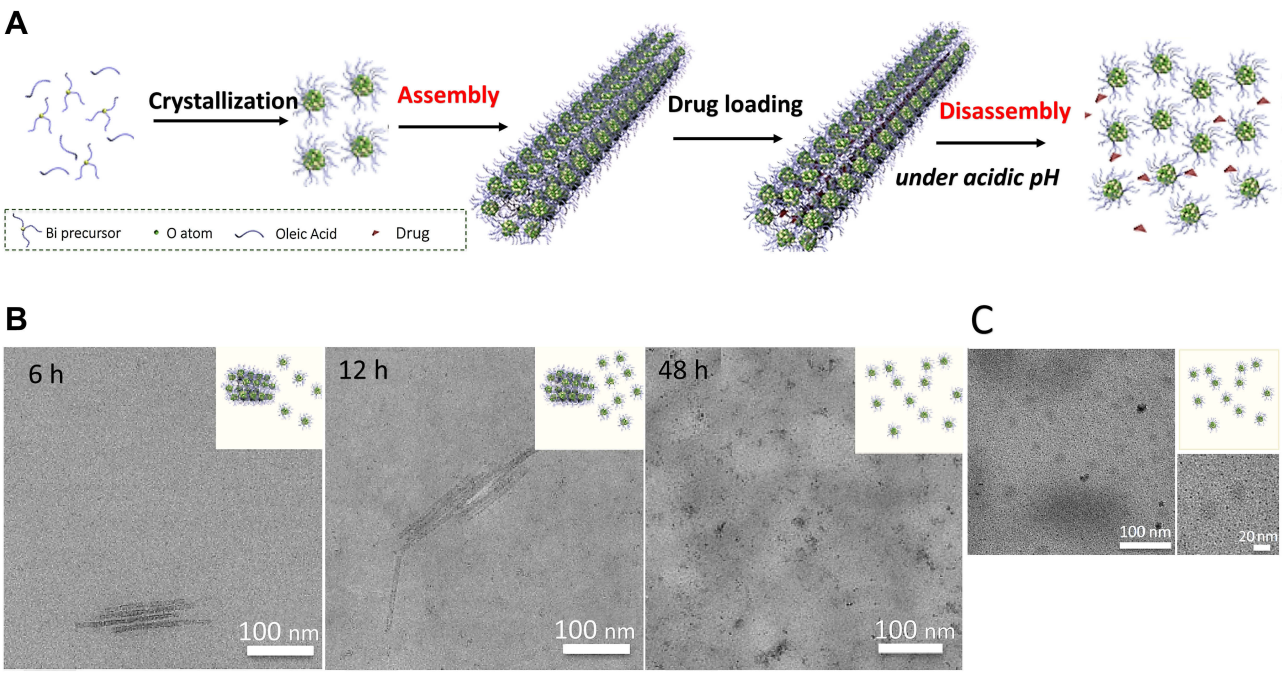

Figure 4 (**A**) Mechanism of the pH-induced disassembly of hollow $(BiO)_2CO_3$ nanotubes (BNTs). (**B**) Transmission electron microscopy (TEM) images of BNTs dispersed in a phosphate buffer saline (PBS) solution (pH 5.5) at different time points. (**C**) TEM images of BNTs in urine collected from a mouse after 3 h. Reprinted with permission from Hu X, Sun J, Li F, et al. Renal-clearable hollow bismuth subcarbonate nanotubes for tumor targeted computed tomography imaging and chemoradiotherapy. *Nano Lett*. 2018;18(2):1196–1204.[81] Copyright 2018, American Chemical Society.

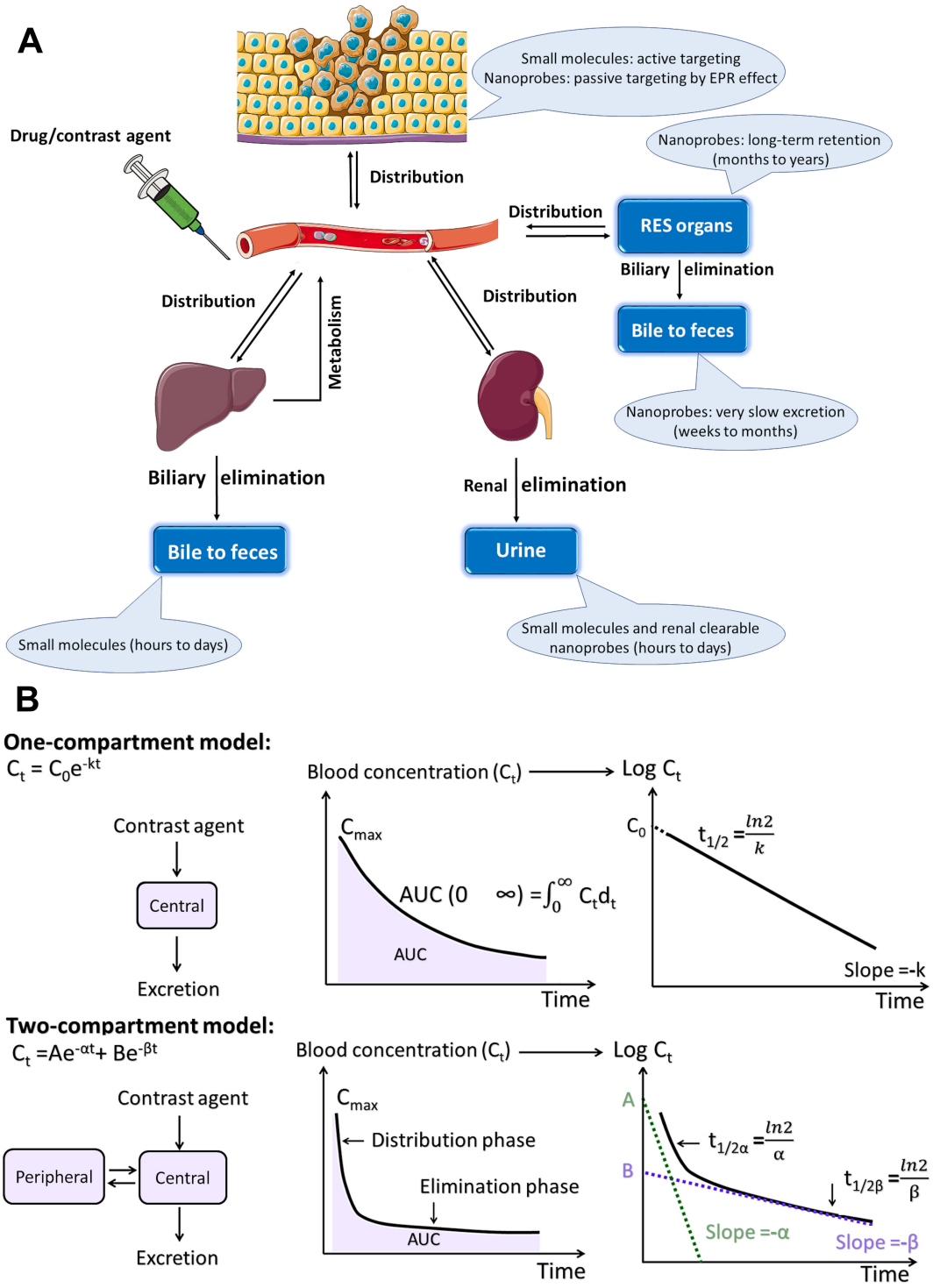

Figure 5 (**A**) Pharmacokinetics (PK) include absorption, distribution, metabolism, and excretion (ADME) of a molecule or nanoprobe. RES: reticuloendothelial system, EPR: enhanced permeability and retention; (**B**) The one-compartment and two-compartment PK models for plotting blood concentration-time curves of a molecule or nanoprobe. Reprinted with permission from Yu M, Zheng J. Clearance pathways and tumor targeting of imaging nanoparticles. *ACS Nano*. 2015;9(7):6655–6674.[76] Copyright 2015, American Chemical Society.

maximum blood concentration (C_{max}), elimination half-life ($t_{1/2}$) and area under the curve (AUC)—can be obtained from the fitted time-dependent concentration curve (Figure 5B), reflecting the quantitative dose amount exposured to the organs and tissues.[76] Additionally, PK parameters not only indicate toxicity but also interestingly

reveal tumor homing capability. To boost the enhanced permeation and retention (EPR) effect and subsequently improve tumor homing efficiency, high blood concentration, long blood clearance half-life and large area under the curve are desirable, due to the passage of nanoprobes from tumor leaky vessels to a tumor extracellular environment as an accumulative process.[82–85]

Based on the previous studies, the PK behavior of Bi NPs has followed either one-compartment or two-compartment models. PEG molecules with an amphiphilic nature are well-known as effective ligands to prolong retention time in the blood; a clearance half-life of ~ 3–5 h was observed in PEGylated Bi NPs with different sizes. An elimination half-life of 3.0, 3.97 and 3.83 h were observed for Bi NCs (HD= 110 nm),[4] Bi NPs (HD= 12 nm)[32] and Bi NPs (HD= 45 nm)[55] with PEG_{5000} coatings, respectively. For PEG_{2000}, the retention time of Gd-Bi NPs in the blood extended to 4.69 h.[58] For Bi_2WO_6-DOX-PEG NPs (117 nm),[11] the blood half-life circulating time was calculated as 3.23 h. The constants of eliminating the rate of Bi_2WO_6-DOX-PEG was calculated as −0.334 μg mL^{-1}. h^{-1} in the first stage, then gradually decreased to −0.019 μg mL^{-1}.h^{-1} in the second stage, also the time interval changes were 2.34 h. The percentage of the volume of Bi_2WO_6-DOX-PEG in the whole blood demonstrates significant increasing distribution kinetics.

HSA also offered long-term circulation in the blood, as the $t_{1/2}$ of 3.8 h was measured for HSA- Bi_2Se_3@PDA NPs (core size of 112 nm).[54] Ultrasound nanocapsules, such as poly (lactic-co-glycolic acid) (PLGA) and perfluorohexane (PFH) carrying Bi_2S_3, had very large hydrodynamic sizes (HD= 754.6 nm and 458.5 nm) and showed a $t_{1/2}$ of 9.44 min (~ 0–2 h p.i.) and 2.2h (~ 0–24 h p.i.), respectively.[86] The circulation times for PVP-Bi NPs were almost the same with a half-life < 2 h, regardless of their sizes. The $t_{1/2}$ of PVP_{1000}- Bi_2Se_3 SSNs (HD= 217 nm) was ~1.7 h.[3] In the case of PVP_{55000}-Bi_2Se_3 nanoplates (HD= 59.8 nm), the concentration of both Bi ($t_{1/2}$= 1.9 h) and Se ($t_{1/2}$= 1.5 h) elements harshly degraded in the first phase, and then Se followed a declining manner with a very low slope, while in contrast, the Bi element concentration was almost steadily up to 70 h.[8] The probes based on small molecules typically have a short distribution half-life ($t_{1/2\alpha}$<0.5 h) and elimination half-life ($t_{1/2\beta}$), followed by a two-compartment model for PK profile and a rapid renal elimination.[76] The $t_{1/2\alpha}$ and $t_{1/2\beta}$ of ultrasmall BSA-Bi_2Se_3 NDs (HD <10 nm) were 0.16 h and 1.49 h, respectively (Figure 6A).[26] Surprisingly, the distribution half-life of the BSA-Bi_2S_3 NPs (HD= 39.5 nm)[28] extended to 14.85 h, which was as long as 10 times than that of BSA-Bi_2Se_3 NDs, while their elimination half-life was found to be 0.78 h.

In the case of $(BiO)_2CO_3$ BNCs embedded into long and hollow $(BiO)_2CO_3$ nanotubes (BNTs),[81] their PK profile followed a two-compartment model that incorporated the benefits of both small molecular probes and nanoprobes (Figure 6B). These advantages include a short distribution half-life ($t_{1/2\alpha}$ = 27.6 min, like small molecular probes <30 min) and very long elimination half-life ($t_{1/2\alpha}$ = 26.99 h) which allowed nanoprobes to flow in the blood at a relatively high level, even 24 h after injection (~ 10% ID•g^{-1}), causing their continuous leakage from the blood vessels into the tumor. The PK profile of BNCs also followed a two-compartment pharmacokinetic model with a $t_{1/2\alpha}$ of 5.4 min and $t_{1/2\beta}$ of 3.77 h (about 7 times shorter than that of the BNTs), during a period of ~ 0–24 h p.i..

PEG can be introduced as a superior choice to modify the surface of nanosystems concerning the following capabilities improving hemo and-cytocompatibility, reducing nonspecific protein adsorption and avoiding opsonization. Thus, PEGylated NPs are retained in the blood circulation for a prolonged time, due to the "stealth" effect of PEG. Nevertheless, clotted blood and anti-PEG immunoglobulin M antibody may occur after the introduction of PEGylated NPs within the body.[87,88]

For the active suppression of this immune attack, the membrane of RBCs as a superior alternative has recently gained attention, due to its countless numbers of glycans, proteins and acidic sialyl moieties. Therefore, the RBC membrane not only merits from biocompatibility, biodegradability, and non-immunogenicity but also the prolonged circulatory residence time of RBC membrane-camouflaged NPs. A superior blood circulation retention time was measured for the RBC membrane-modified Bi NPs[53] in comparison to unmodified ones, indicating the major role of the RBC membrane to decrease macrophage uptake, delay clearance and prolong circulation time. In contrast, there was no contribution to folate modification—a similar blood circulation period as the ones modified with RBC only was found for folate functional RBC-membrane-modified Bi NPs (F-RBC Bi NPs). The blood retention time of RBC membrane-coated Bi NPs was considerably extended as high as over 24 h, and their blood content was ~11% ID•g^{-1} even at 24 h after injection, over 9-times larger

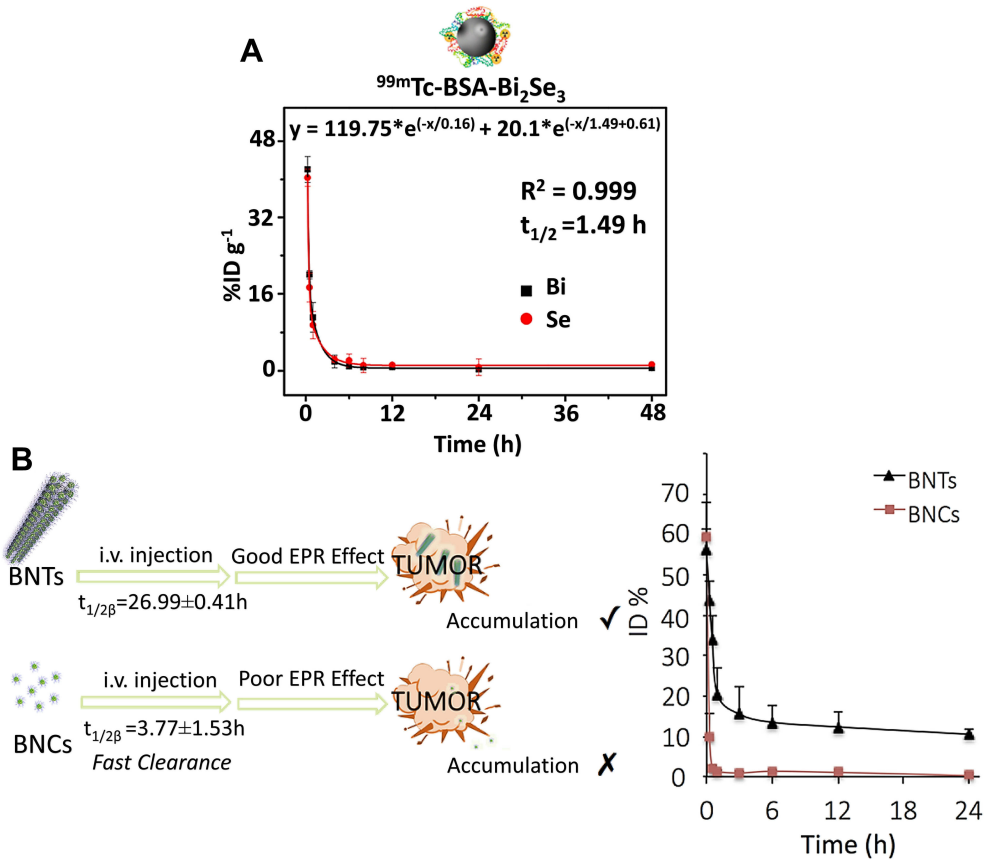

Figure 6 (**A**) Blood circulation profile of bovine serum albumin coated bismuth selenide nanoparticles (BSA-Bi_2S_3 NPs) in mice fitted with a two-compartment model. Reprinted with permission from Mao F, Wen L, Sun C, et al. Ultrasmall biocompatible Bi2Se3 nanodots for multimodal imaging-guided synergistic radiophotothermal therapy against cancer. *ACS Nano*. 2016;10(12):11145–11155.[26] Copyright 2016, American Chemical Society. (**B**) Blood circulation profile of bismuth (Bi) concentration in the hollow $(BiO)_2CO_3$ nanotubes (BNTs) and $(BiO)_2CO_3$ nanoclusters (BNCs) in mice fitted with a two-compartment model. Reprinted with permission from Hu X, Sun J, Li F, et al. Renal-clearable hollow bismuth subcarbonate nanotubes for tumor targeted computed tomography imaging and chemoradiotherapy. *Nano Lett*. 2018;18(2):1196–1204.[81] Copyright 2018, American Chemical Society.

than unmodified ones. These PK parameters of contrast agents can quantitatively reflect the exposure of organs and tissues to the agents and affect not only toxicity but also tumor targeting efficiency.[76]

Conclusions and Prospects

Nanotechnology and nanomaterials are inevitable parts of the modern, improved, and innovative scenarios in industrial and biomedical applications. Nanomaterials with their unique, tailored, and size-dependent properties endow brilliant features to conventional materials. They can alter and induce desired effects in very low quantities in comparison to the bulk material; it is why they have attracted considerable attention. In this regard, it is critical to assess the fate of nanomaterials within the human body and provide suitable and specific guidelines toward their application and handling. It is critical to evaluate exposure routes, interactions with biological systems, pharmacokinetics, and clearance routes of nanostructures. Moreover, since every type of nanostructure has its own mode of action, the above-mentioned issues should be assessed for each individual nanostructure.

Bi-based components have a long history in medicine especially due to their antimicrobial activities. With the advent of nanotechnology, considerable attention has been paid to nanostructured bismuth, their properties, and applications. Various studies conducted along with this concept and their pros and cons were documented in this unique review. However, there has been a lack of a comprehensive review evaluating their mode of action within the human body. Various studies reported high biocompatibility and, interestingly, optimal biodegradability of BiNPs for medical applications. It is shown that dissolved Bi (III) ions from BiNPs are cleared via metallothionine, a cysteine-rich protein in kidneys, and excerted by urine. Bi-based nanocompounds exhibited excellent blood compatibility with a hemolysis

effect lower than 2%, even at a high concentration of 800 $\mu g \bullet mL^{-1}$. The physical states of the animal models were monitored after the administration of BiNPs and the results showed no significant weight loss. Also, it has been reported that no obvious abnormal behavior was observed after treatment, indicating physically and behaviorally excellent in vivo compatibility of BiNPs. In addition to the physical signs, histological evaluations confirmed that BiNPs with various shapes, coatings, and compounds did not induce any significant tissue damage and all major organs (heart, liver, spleen, lung, and kidney) maintained normal physiological properties.

Since most of the prepared and evaluated BiNPs were larger than FST, they followed a non-renal clearance profile and demonstrated liver homing in the range of 8 ~ 70% $ID \bullet g^{-1}$ at 1 ~ 24 h p.i. with any shape, hydrodynamic size (larger than FST), surface coating and chemical composition. Even though various studies have been conducted to assess the fate of BiNPs in the human body, protein corona formation details have been neglected so far. Protein corona formation, its status, and dynamics are critical parameters determining the fate of NPs and the effectiveness of the proposed medical application. According to the authors' opinion, it is essential to assess and control the protein corona using simulation and experimental studies. In conclusion, Bi-based nanostructures exhibited beneficial properties and can be considered as a promising diagnostic, therapeutic, and even theranostic agent.

Acknowledgments

The authors gratefully acknowledge the financial support from Kermanshah University of Medical Sciences, Kermanshah, Iran (Grant No. 980440).

Disclosure

The authors report no conflicts of interest in this work.

References

1. Lei P, An R, Zhang P, et al. Ultrafast synthesis of ultrasmall poly (Vinylpyrrolidone)-protected bismuth nanodots as a multifunctional theranostic agent for in vivo dual-modal CT/Photothermal-imaging-guided photothermal therapy. *Adv Funct Mater*. 2017;27(35):35.
2. Li Z, Hu Y, Chang M, et al. Highly porous PEGylated Bi 2 S 3 nano-urchins as a versatile platform for in vivo triple-modal imaging, photothermal therapy and drug delivery. *Nanoscale*. 2016;8 (35):16005–16016. doi:10.1039/C6NR03398A
3. Li Z, Liu J, Hu Y, et al. Multimodal imaging-guided antitumor photothermal therapy and drug delivery using bismuth selenide spherical sponge. *ACS Nano*. 2016;10(10):9646–9658. doi:10.1021/acsnano.6b05427
4. Li Z, Liu J, Hu Y, et al. Biocompatible PEGylated bismuth nanocrystals:"All-in-one" theranostic agent with triple-modal imaging and efficient in vivo photothermal ablation of tumors. *Biomaterials*. 2017;141:284–295. doi:10.1016/j.biomaterials.2017.06.033
5. Zhou S-M, Ma D-K, Zhang S-H, et al. PEGylated Cu 3 BiS 3 hollow nanospheres as a new photothermal agent for 980 nm-laser-driven photothermochemotherapy and a contrast agent for X-ray computed tomography imaging. *Nanoscale*. 2016;8(3):1374–1382. doi:10.1039/C5NR06041A
6. Dou R, Du Z, Bao T, et al. The polyvinylpyrrolidone functionalized rGO/Bi 2 S 3 nanocomposite as a near-infrared light-responsive nanovehicle for chemo-photothermal therapy of cancer. *Nanoscale*. 2016;8(22):11531–11542. doi:10.1039/C6NR01543C
7. Du J, Gu Z, Yan L, et al. Poly (Vinylpyrollidone)-and Selenocysteine-Modified Bi2Se3 Nanoparticles Enhance Radiotherapy Efficacy in Tumors and Promote Radioprotection in Normal Tissues. *Advan Mater*. 2017;29:34.
8. Zhang XD, Chen J, Min Y, et al. Metabolizable Bi2Se3 nanoplates: biodistribution, toxicity, and uses for cancer radiation therapy and imaging. *Adv Funct Mater*. 2014;24(12):1718–1729. doi:10.1002/adfm.201302312
9. Cheng L, Shen S, Shi S, et al. FeSe2-decorated Bi2Se3 nanosheets fabricated via cation exchange for chelator-free 64Cu-labeling and multimodal image-guided photothermal-radiation therapy. *Adv Funct Mater*. 2016;26(13):2185–2197. doi:10.1002/adfm.201504810
10. Yang C, Chen Y, Guo W, et al. Bismuth ferrite-based nanoplatform design: an ablation mechanism study of solid tumor and NIR-triggered photothermal/photodynamic combination cancer therapy. *Adv Funct Mater*. 2018;28(18):1706827. doi:10.1002/adfm.201706827
11. Feng L, Yang D, Gai S, et al. Single bismuth tungstate nanosheets for simultaneous chemo-, photothermal, and photodynamic therapies mediated by near-infrared light. *Chem Eng J*. 2018;351:1147–1158. doi:10.1016/j.cej.2018.06.170
12. Badrigilan S, Choupani J, Khanbabaei H, Hoseini-Ghahfarokhi M, Webster TJ, Tayeri L. Bismuth-based nanomaterials: Recent advances in tumor targeting and synergistic cancer therapy techniques. *Adv Healthc Mater*. 2020;9(7):1901695. doi:10.1002/adhm.201901695
13. Choi HS, Liu W, Misra P, et al. Renal clearance of quantum dots. *Nat Biotechnol*. 2007;25(10):1165. doi:10.1038/nbt1340
14. Khlebtsov N, Dykman L. Biodistribution and toxicity of engineered gold nanoparticles: a review of in vitro and in vivo studies. *Chem Soc Rev*. 2011;40(3):1647–1671. doi:10.1039/C0CS00018C
15. Arami H, Khandhar A, Liggitt D, Krishnan KM. In vivo delivery, pharmacokinetics, biodistribution and toxicity of iron oxide nanoparticles. *Chem Soc Rev*. 2015;44(23):8576–8607. doi:10.1039/C5CS00541H
16. Sukhanova A, Bozrova S, Sokolov P, Berestovoy M, Karaulov A, Nabiev I. Dependence of nanoparticle toxicity on their physical and chemical properties. *Nanoscale Res Lett*. 2018;13(1):44. doi:10.1186/s11671-018-2457-x
17. Mohan R. Green bismuth. *Nat Chem*. 2010;2(4):336. doi:10.1038/nchem.609
18. Brown AL, Naha PC, Benavides-Montes V, Litt HI, Goforth AM, Cormode DP. Synthesis, X-ray opacity, and biological compatibility of ultra-high payload elemental bismuth nanoparticle X-ray contrast agents. *Chem Mater*. 2014;26(7):2266–2274. doi:10.1021/cm500077z
19. Briand GG, Burford N. Bismuth compounds and preparations with biological or medicinal relevance. *Chem Rev*. 1999;99(9):2601–2658. doi:10.1021/cr980425s
20. Mjos KD, Orvig C. Metallodrugs in medicinal inorganic chemistry. *Chem Rev*. 2014;114(8):4540–4563. doi:10.1021/cr400460s
21. Gorbach SL. Bismuth therapy in gastrointestinal diseases. *Gastroenterology*. 1990;99(3):863–875. doi:10.1016/0016-5085(90)90983-8

22. Sun H, Li H, Harvey I, Sadler PJ. Interactions of bismuth complexes with metallothionein (II). *J Biol Chem*. 1999;274(41):29094–29101. doi:10.1074/jbc.274.41.29094
23. Veintemillas-Verdaguer S, Luengo Y, Serna C, et al. Bismuth labeling for the CT assessment of local administration of magnetic nanoparticles. *Nanotechnology*. 2015;26(13):135101. doi:10.1088/0957-4484/26/13/135101
24. Liu J, Zheng X, Yan L, et al. Bismuth sulfide nanorods as a precision nanomedicine for in vivo multimodal imaging-guided photothermal therapy of tumor. *ACS Nano*. 2015;9(1):696–707. doi:10.1021/nn506137n
25. Ma M, Huang Y, Chen H, et al. Bi2S3-embedded mesoporous silica nanoparticles for efficient drug delivery and interstitial radiotherapy sensitization. *Biomaterials*. 2015;37:447–455. doi:10.1016/j.biomaterials.2014.10.001
26. Mao F, Wen L, Sun C, et al. Ultrasmall biocompatible Bi2Se3 nanodots for multimodal imaging-guided synergistic radiophotothermal therapy against cancer. *ACS Nano*. 2016;10(12):11145–11155. doi:10.1021/acsnano.6b06067
27. Naha PC, Al Zaki A, Hecht E, et al. Dextran coated bismuth–iron oxide nanohybrid contrast agents for computed tomography and magnetic resonance imaging. *J Mater Chem B*. 2014;2(46):8239–8248. doi:10.1039/C4TB01159G
28. Wang Y, Wu Y, Liu Y, et al. BSA-mediated synthesis of bismuth sulfide nanotheranostic agents for tumor multimodal imaging and thermoradiotherapy. *Adv Funct Mater*. 2016;26(29):5335–5344. doi:10.1002/adfm.201601341
29. Li A, Li X, Yu X, et al. Synergistic thermoradiotherapy based on PEGylated Cu3BiS3 ternary semiconductor nanorods with strong absorption in the second near-infrared window. *Biomaterials*. 2017;112:164–175. doi:10.1016/j.biomaterials.2016.10.024
30. Wei B, Zhang X, Zhang C, et al. Facile synthesis of uniform-sized bismuth nanoparticles for CT visualization of gastrointestinal tract in vivo. *ACS Appl Mater Interfaces*. 2016;8(20):12720–12726. doi:10.1021/acsami.6b03640
31. Yang Y, Wu H, Shi B, et al. Hydrophilic Cu3BiS3 nanoparticles for computed tomography imaging and photothermal therapy. *Particle Particle Syst Charact*. 2015;32(6):668–679. doi:10.1002/ppsc.201400238
32. Yu X, Li A, Zhao C, Yang K, Chen X, Li W. Ultrasmall semimetal nanoparticles of bismuth for dual-modal computed tomography/photoacoustic imaging and synergistic thermoradiotherapy. *ACS Nano*. 2017;11(4):3990–4001. doi:10.1021/acsnano.7b00476
33. Zhang Y, Zhang H, Wang Y, et al. Hydrophilic graphene oxide/bismuth selenide nanocomposites for CT imaging, photoacoustic imaging, and photothermal therapy. *J Mater Chem B*. 2017;5(9):1846–1855. doi:10.1039/C6TB02137A
34. Badrigilan S, Shaabani B, Gharehaghaji N, Mesbahi A. Iron oxide/bismuth oxide nanocomposites coated by graphene quantum dots:"Three-in-one" theranostic agents for simultaneous CT/MR imaging-guided in vitro photothermal therapy. *Photodiagnosis Photodyn Ther*. 2019;25:504–514. doi:10.1016/j.pdpdt.2018.10.021
35. Badrigilan S, Shaabani B, Aghaji NG, Mesbahi A. Graphene quantum dots-coated bismuth nanoparticles for improved CT imaging and photothermal performance. *Int J Nanosci*. 2018;1850043.
36. Liu Y, Zhuang J, Zhang X, et al. Autophagy associated cytotoxicity and cellular uptake mechanisms of bismuth nanoparticles in human kidney cells. *Toxicol Lett*. 2017;275:39–48. doi:10.1016/j.toxlet.2017.04.014
37. Rabin O, Perez JM, Grimm J, Wojtkiewicz G, Weissleder R. An X-ray computed tomography imaging agent based on long-circulating bismuth sulphide nanoparticles. *Nat Mater*. 2006;5(2):118–122. doi:10.1038/nmat1571
38. Abudayyak M, Öztaş E, Arici M, Özhan G. Investigation of the toxicity of bismuth oxide nanoparticles in various cell lines. *Chemosphere*. 2017;169:117–123. doi:10.1016/j.chemosphere.2016.11.018
39. Gao X, Zhang X, Wang Y, Wang Y, Peng S, Fan C. An in vitro study on the cytotoxicity of bismuth oxychloride nanosheets in human HaCaT keratinocytes. *Food Chem Toxicol*. 2015;80:52–61. doi:10.1016/j.fct.2015.02.018
40. Gao X, Wang Y, Peng S, et al. Comparative toxicities of bismuth oxybromide and titanium dioxide exposure on human skin keratinocyte cells. *Chemosphere*. 2015;135:83–93. doi:10.1016/j.chemosphere.2015.03.075
41. Ai K, Liu Y, Liu J, Yuan Q, He Y, Lu L. Large-scale synthesis of Bi2S3 nanodots as a contrast agent for in vivo X-ray computed tomography imaging. *Advan Mater*. 2011;23(42):4886–4891. doi:10.1002/adma.201103289
42. Cornélio ALG, Salles LP, da Paz MC, Cirelli JA, Guerreiro-Tanomaru JM, Tanomaru Filho M. Cytotoxicity of Portland cement with different radiopacifying agents: a cell death study. *J Endod*. 2011;37(2):203–210. doi:10.1016/j.joen.2010.11.017
43. Hernandez-Delgadillo R, Velasco-Arias D, Martinez-Sanmiguel JJ, et al. Bismuth oxide aqueous colloidal nanoparticles inhibit Candida albicans growth and biofilm formation. *Int J Nanomedicine*. 2013;8:1645. doi:10.2147/IJN.S37465
44. Wang Y, Cai D, Wu H, et al. Functionalized Cu 3 BiS 3 nanoparticles for dual-modal imaging and targeted photothermal/photodynamic therapy. *Nanoscale*. 2018;10(9):4452–4462. doi:10.1039/C7NR07458A
45. Du J, Zheng X, Yong Y, et al. Design of TPGS-functionalized Cu 3 BiS 3 nanocrystals with strong absorption in the second near-infrared window for radiation therapy enhancement. *Nanoscale*. 2017;9(24):8229–8239. doi:10.1039/C7NR02213A
46. Du F, Lou J, Jiang R, et al. Hyaluronic acid-functionalized bismuth oxide nanoparticles for computed tomography imaging-guided radiotherapy of tumor. *Int J Nanomedicine*. 2017;12:5973. doi:10.2147/IJN.S130455
47. Yang S, Li Z, Wang Y, et al. Multifunctional Bi@ PPy-PEG core–shell nanohybrids for dual-modal imaging and photothermal therapy. *ACS Appl Mater Interfaces*. 2018;10(2):1605–1615. doi:10.1021/acsami.7b17838
48. Liu J, Wang P, Zhang X, et al. Rapid degradation and high renal clearance of Cu3BiS3 nanodots for efficient cancer diagnosis and photothermal therapy in vivo. *ACS Nano*. 2016;10(4):4587–4598. doi:10.1021/acsnano.6b00745
49. Du J, Wang X, Dong X, et al. Enhanced radiosensitization of ternary Cu 3 BiSe 3 nanoparticles by photo-induced hyperthermia in the second near-infrared biological window. *Nanoscale*. 2019;11(15):7157–7165. doi:10.1039/C8NR09618J
50. Yu H, Yang Y, Jiang T, et al. Effective radiotherapy in tumor assisted by ganoderma lucidum polysaccharide-conjugated bismuth sulfide nanoparticles through radiosensitization and dendritic cell activation. *ACS Appl Mater Interfaces*. 2019;11(31):27536–27547. doi:10.1021/acsami.9b07804
51. Xie H, Li Z, Sun Z, et al. Metabolizable Ultrathin Bi2Se3 nanosheets in imaging-guided photothermal therapy. *Small*. 2016;12(30):4136–4145. doi:10.1002/smll.201601050
52. Li J, Jiang F, Yang B, et al. Topological insulator bismuth selenide as a theranostic platform for simultaneous cancer imaging and therapy. *Sci Rep*. 2013;3(1):1–7.
53. Deng J, Xu S, Hu W, Xun X, Zheng L, Su M. Tumor targeted, stealthy and degradable bismuth nanoparticles for enhanced X-ray radiation therapy of breast cancer. *Biomaterials*. 2018;154:24–33. doi:10.1016/j.biomaterials.2017.10.048
54. Läubli H, Balmelli C, Bossard M, Pfister O, Glatz K, Zippelius A. Acute heart failure due to autoimmune myocarditis under pembrolizumab treatment for metastatic melanoma. *J Immunother Cancer*. 2015;3(1):11. doi:10.1186/s40425-015-0057-1
55. Kinsella JM, Jimenez RE, Karmali PP, et al. X-ray computed tomography imaging of breast cancer by using targeted peptide-labeled bismuth sulfide nanoparticles. *Angewandte Chemie Int Ed*. 2011;50(51):12308–12311. doi:10.1002/anie.201104507

56. Cheng Y, Chang Y, Feng Y, Jian H, Tang Z, Zhang H. Deep-Level defect enhanced photothermal performance of bismuth sulfide–gold heterojunction nanorods for photothermal therapy of cancer guided by computed tomography imaging. *Angewandte Chemie Int Ed*. 2018;57(1):246–251. doi:10.1002/anie.201710399
57. Xu Y, Shi Z, Brown EMB, Wu A. Layered bismuth oxyhalide nanomaterials for highly efficient tumor photodynamic therapy. *Nanoscale*. 2016;8(25):12715–12722. doi:10.1039/C5NR04540A
58. Wu B, Lu S-T, Yu H, et al. Gadolinium-chelate functionalized bismuth nanotheranostic agent for in vivo MRI/CT/PAI imaging-guided photothermal cancer therapy. *Biomaterials*. 2018;159:37–47. doi:10.1016/j.biomaterials.2017.12.022
59. Yang D, Yang G, Li J, Gai S, He F, Yang P. NIR-driven water splitting by layered bismuth oxyhalide sheets for effective photodynamic therapy. *J Mater Chem B*. 2017;5(22):4152–4161. doi:10.1039/C7TB00688H
60. Lei P, Zhang P, Yuan Q, et al. Yb3+/Er3+-Codoped Bi2O3 Nanospheres: probe for Upconversion Luminescence Imaging and Binary Contrast Agent for Computed Tomography Imaging. *ACS Appl Mater Interfaces*. 2015;7(47):26346–26354. doi:10.1021/acsami.5b09990
61. Zang Y, Gong L, Mei L, Gu Z, Wang Q. Bi2WO6 semiconductor nanoplates for tumor radiosensitization through high-Z effects and radiocatalysis. *ACS Appl Mater Interfaces*. 2019;11(21):18942–18952. doi:10.1021/acsami.9b03636
62. Xiong Y, Sun F, Liu P, et al. A biomimetic one-pot synthesis of versatile Bi2S3/FeS2 theranostic nanohybrids for tumor-targeted photothermal therapy guided by CT/MR dual-modal imaging. *Chem Eng J*. 2019;378:122172. doi:10.1016/j.cej.2019.122172
63. Kandanapitiye MS, Gao M, Molter J, Flask CA, Huang SD. Synthesis, characterization, and X-ray attenuation properties of ultrasmall BiOI nanoparticles: toward renal clearable particulate CT contrast agents. *Inorg Chem*. 2014;53(19):10189–10194. doi:10.1021/ic5011709
64. Chen Y, Zhao G, Wang S, et al. Platelet-membrane-camouflaged bismuth sulfide nanorods for synergistic radio-photothermal therapy against cancer. *Biomater Sci*. 2019;7(8):3450–3459. doi:10.1039/C9BM00599D
65. Wang X, Guo Z, Zhang C, et al. Ultrasmall BiOI quantum dots with efficient renal clearance for enhanced radiotherapy of cancer. *Advan Sci*. 2020;7(6):1902561. doi:10.1002/advs.201902561
66. An R, Lei P, Zhang P, Xu X, Feng J, Zhang H. Near-infrared optical and X-ray computed tomography dual-modal imaging probe based on novel lanthanide-doped K 0.3 Bi 0.7 F 2.4 upconversion nanoparticles. *Nanoscale*. 2018;10:3. doi:10.1039/C7NR06758E
67. Xu L, He F, Wang C, et al. Lanthanide-doped bismuth oxobromide nanosheets for self-activated photodynamic therapy. *J Mater Chem B*. 2017;5(39):7939–7948. doi:10.1039/C7TB01983A
68. Zhang L, Chen Q, Zou X, et al. Intelligent protein-coated bismuth sulfide and manganese oxide nanocomposites obtained by biomineralization for multimodal imaging-guided enhanced tumor therapy. *J Mater Chem B*. 2019;7(34):5170–5181. doi:10.1039/C9TB00991D
69. Cheng J, Wang W, Xu X, et al. AgBiS2 nanoparticles with synergistic photodynamic and bioimaging properties for enhanced malignant tumor phototherapy. *Mater Sci Eng*. 2020;107:110324. doi:10.1016/j.msec.2019.110324
70. Cheng Y, Chang Y, Feng Y, et al. Bismuth sulfide nanorods with retractable zinc protoporphyrin molecules for suppressing innate antioxidant defense system and strengthening phototherapeutic effects. *Advan Mater*. 2019;31(10):1806808. doi:10.1002/adma.201806808
71. Aviv H, Bartling S, Grinberg I, Margel S. Synthesis and characterization of Bi2O3/HSA core-shell nanoparticles for X-ray imaging applications. *J Biomed Mater Res B Appl Biomater*. 2013;101(1):131–138. doi:10.1002/jbm.b.32826
72. Zheng X, Shi J, Bu Y, et al. Silica-coated bismuth sulfide nanorods as multimodal contrast agents for a non-invasive visualization of the gastrointestinal tract. *Nanoscale*. 2015;7(29):12581–12591. doi:10.1039/C5NR03068D
73. He N, Li X, Feng D, et al. Exploring the toxicity of a bismuth–asparagine coordination polymer on the early development of zebrafish embryos. *Chem Res Toxicol*. 2013;26(1):89–95. doi:10.1021/tx3004032
74. Zhang X-D, Jing Y, Song S, et al. Catalytic topological insulator Bi2Se3 nanoparticles for in vivo protection against ionizing radiation. *Nanomedicine*. 2017;13(5):1597–1605. doi:10.1016/j.nano.2017.02.018
75. Lei P, An R, Zhang P, et al. Ultrafast synthesis of ultrasmall poly (Vinylpyrrolidone)-protected Bismuth Nanodots as a multifunctional theranostic agent for in vivo dual-modal CT/Photothermal-imaging-guided photothermal therapy. *Adv Funct Mater*. 2017;27(35):1702018.
76. Yu M, Zheng J. Clearance pathways and tumor targeting of imaging nanoparticles. *ACS Nano*. 2015;9(7):6655–6674. doi:10.1021/acsnano.5b01320
77. Yu N, Wang Z, Zhang J, et al. Thiol-capped Bi nanoparticles as stable and all-in-one type theranostic nanoagents for tumor imaging and thermoradiotherapy. *Biomaterials*. 2018;161:279–291. doi:10.1016/j.biomaterials.2018.01.047
78. Du J, Gu Z, Yan L, et al. Poly (Vinylpyrollidone)-and selenocysteine-modified Bi2Se3 nanoparticles enhance radiotherapy efficacy in tumors and promote radioprotection in normal tissues. *Advan Mater*. 2017;29(34):1701268.
79. Walkey CD, Olsen JB, Guo H, Emili A, Chan WC. Nanoparticle size and surface chemistry determine serum protein adsorption and macrophage uptake. *J Am Chem Soc*. 2012;134(4):2139–2147. doi:10.1021/ja2084338
80. Lynch I, Dawson KA. Protein-nanoparticle interactions. *Nano Today*. 2008;3(1–2):40–47. doi:10.1016/S1748-0132(08)70014-8
81. Hu X, Sun J, Li F, et al. Renal-clearable hollow bismuth subcarbonate nanotubes for tumor targeted computed tomography imaging and chemoradiotherapy. *Nano Lett*. 2018;18(2):1196–1204. doi:10.1021/acs.nanolett.7b04741
82. Zhang G, Yang Z, Lu W, et al. Influence of anchoring ligands and particle size on the colloidal stability and in vivo biodistribution of polyethylene glycol-coated gold nanoparticles in tumor-xenografted mice. *Biomaterials*. 2009;30(10):1928–1936. doi:10.1016/j.biomaterials.2008.12.038
83. Liu J, Yu M, Ning X, Zhou C, Yang S, Zheng J. PEGylation and zwitterionization: pros and cons in the renal clearance and tumor targeting of near-IR-emitting gold nanoparticles. *Angewandte Chemie*. 2013;125(48):12804–12808. doi:10.1002/ange.201304465
84. Arvizo RR, Miranda OR, Moyano DF, et al. Modulating pharmacokinetics, tumor uptake and biodistribution by engineered nanoparticles. *PLoS One*. 2011;6(9):e24374. doi:10.1371/journal.pone.0024374
85. Li S-D, Huang L. Pharmacokinetics and biodistribution of nanoparticles. *Mol Pharm*. 2008;5(4):496–504. doi:10.1021/mp800049w
86. Zhou D, Li C, He M, et al. Folate-targeted perfluorohexane nanoparticles carrying bismuth sulfide for use in US/CT dual-mode imaging and synergistic high-intensity focused ultrasound ablation of cervical cancer. *J Mater Chem B*. 2016;4(23):4164–4181. doi:10.1039/C6TB00261G
87. Armstrong JK, Hempel G, Koling S, et al. Antibody against poly (ethylene glycol) adversely affects PEG-asparaginase therapy in acute lymphoblastic leukemia patients. *Cancer*. 2007;110(1):103–111. doi:10.1002/cncr.22739
88. Garay RP, El-Gewely R, Armstrong JK, Garratty G, Richette P. *Antibodies Against Polyethylene Glycol in Healthy Subjects and in Patients Treated with PEG-Conjugated Agents*. Taylor & Francis; 2012.